Symmetry forbidden vibronic spectra and internal conversion in benzene

Jun Li,[a] Chih-Kai Lin,*[bc] Xiang Yuan Li,*[a] Chao Yuan Zhu[c] and Sheng Hsien Lin[bc]

Received 4th April 2010, Accepted 25th August 2010
DOI: 10.1039/c0cp00120a

The spectra of symmetry-forbidden transitions and internal conversion were investigated in the present work. Temperature dependence was taken into account for the spectra simulation. The vibronic coupling, essential in the two processes, was calculated based on the Herzberg–Teller theory within the Born–Oppenheimer approximation. The approach was employed for the symmetry-forbidden absorption/fluorescence, and internal conversion between 1^1A_{1g} and 1^1B_{2u} states in benzene. Vibrational frequencies, normal coordinates, electronic transition dipole moments, and non-adiabatic coupling matrix elements were obtained by *ab initio* quantum chemical methods. The main peaks, along with the weak peaks, were in good agreement with the observed ones. The rate constant of the $1^1A_{1g} \leftarrow 1^1B_{2u}$ internal conversion was estimated within the order of 10^3 s^{-1}. This could be regarded as the lower limit (about 4.8×10^3 s^{-1}) of the internal conversion. It is stressed that the distortion effect was taken into account both in the symmetry-forbidden absorption/fluorescence, and the rate constants of internal conversion in the present work. The distortion effects complicate the spectra and increase the rate constants of internal conversion.

Introduction

The coupling between the electronic and nuclear motions in molecules alias vibronic coupling is of great importance in molecular spectroscopy, photochemical reactions, biological processes, and laser technology. For example, the observation of the weak symmetry-forbidden transitions in absorption and fluorescence spectra is caused by vibronic coupling: it can "borrow" intensities from other intermediate allowed states through certain normal modes of a particular symmetry, *i.e.* the "promoting mode". Also, IC (internal conversion), defined as the radiationless transitions of electronic states of like multiplicity, involves the vibronic coupling. In this process, the electronic excitation energy is transformed into the vibrational energy of the electronic ground state.[1]

Using the perturbation method, Herzberg and Teller[2] illustrated the principles of the vibronic coupling and the intensity of symmetry-forbidden transitions. From that, one can determine which normal modes will make transitions allowed, and how to obtain intensities from the electronic wave functions at its equilibrium. In this picture, the electronic and nuclear wave functions are completely decoupled in the zeroth-order approximations. Therefore the allowed vibronic transitions arise due to the interaction between electronic and nuclear motion. Thus, only some modes of a particular symmetry can induce the transitions according to the symmetry rule. This intensity-borrowing is effective when the borrowing band is close to the symmetry-allowed band in energy. On the other hand, the first derivatives of the transition dipole moment along the normal coordinates can be directly calculated by the finite difference method. Roos *et al.*[3] expressed the wave functions as a function of a perturbation strength to obtain derivatives of the transition properties, and then employ this method to calculate the vibronic coupling for symmetry-forbidden transitions in benzene. Borges *et al.*[4] expanded the transition dipole moments as a power series assuming that the total transition dipole moment is the sum of the transition dipole moments along each participating mode. The vibronic coupling can be obtained by the Herzberg–Teller theory or directly by the numerical method. The former is adopted in the present work since the major inaccuracy may not come from approximations in the theory but from computational methods. It is because that the algorithms used to compute excited states are not as efficient as for ground states and it is even harder to calculate reliable derivatives of the transition properties.

Once the vibronic coupling is known, we have to calculate the Franck–Condon (FC) overlap integrals of vibrational wave functions of the two electronic states. FC integrals are essential in the theoretical description for the vibronic structure of electronic spectra like absorption and fluorescence, as well as other nonradiative processes such as internal conversion. However, exact calculation for multidimensional FC integrals is impractical for large polyatomic molecules. Within the harmonic or anharmonic framework, further approximations such as displaced oscillator model, distorted oscillator model, and the mode-mixing effect or the Duschinsky effect can be introduced. Though a great deal of theoretical works[1,6–10] have been done on IC, practical calculations based on *ab initio* wave functions are still scarce. In the present work, we have considered the distorted

[a] *College of Chemical Engineering, Sichuan University, Chengdu 610065, China. E-mail: xyli@scu.edu.cn*
[b] *Institute of Atomic and Molecular Sciences, Academia Sinica, Taipei 10617, Taiwan. E-mail: ethene@gate.sinica.edu.tw*
[c] *Department of Applied Chemistry, Institute of Molecular Science and Center for Interdisciplinary Molecular Science, National Chiao-Tung University, 1001 Ta-Hsueh Rd., Hsinchu 300, Taiwan*

oscillator effect in spectrum simulation and the rate constants of the IC based on the *ab initio* computation of the vibronic coupling.

Benzene and its derivatives form a basic structure for a vast range of organic compounds in nature, and can therefore be considered as a model compound for a wide variety of hydrocarbons. Despite being a simple molecule, benzene has been the subject of many theoretical and experimental investigations.[11–29] With 30 vibrational degrees of freedom, benzene is of the D_{6h} point group, giving unusual theoretical accessibility. Its transition from the $^1A_{1g}$ ground state to the low-lying $^1B_{2u}$ excited state is one-photon symmetry-forbidden. The spectra of this absorption, though very weak, have a relatively small number of lines. In other words, they are distinguishable. Klessinger *et al.*[27] implemented the program HOTFCHT to simulate the absorption and fluorescence spectra for the transition in benzene. They considered the temperature effect, the anharmonic effect, the Duschinsky effect and so on. Roos *et al.*[3] also presented simulation on the vibronic spectra of this transition. However, theoretical research for IC of benzene is still rare.

The present work is outlined as follows: In the Theory section, the fundamental formulation of the absorption spectrum and fluorescence for symmetry-forbidden transitions and rate constants of the IC are derived. In the Results and discussion, the first symmetry-forbidden transition in benzene is investigated by the approach given in the Theory section based on results from *ab initio* methods. The simulated absorption and fluorescence spectra between the two states are reported. This section also presents calculations of rate constants of IC for this transition. It is emphasized that the distorted oscillator effect is considered. The Conclusions section gives the concluding remarks of the present work.

Theory

Spectra for symmetry forbidden transitions

The transition processes can be described using the time-dependent Schrödinger equation. Its Hamiltonian consists of two parts: the zeroth order Hamiltonian $\hat{H}_0$, which denotes the stationary properties of the molecule system, and the perturbation term $\hat{H}'$, which is responsible for the transition process under consideration. If the perturbation term is small, the problem can be solved by the perturbation method.

For the optical absorption processes, the perturbation is time-dependent. The absorption coefficient $\alpha(\omega)$ in the gas phase for a transition from the electronic initial state a to the final state b takes the form[30,31]

$$\alpha(\omega) = \frac{4\pi^2\omega}{3\hbar c}\sum_{av}\sum_{bv'} P_{av}|\langle\varphi_{bv'}|\vec{\mu}|\varphi_{av}\rangle|^2 D(\omega_{bv',av}-\omega) \quad (1)$$

by means of the first-order perturbation method, which corresponds to the one-photon absorption. In eqn (1), P_{av} is the Boltzmann distribution function of the initial vibrational state at temperature T, φ_{av} and $\varphi_{bv'}$ represent the molecular wave functions with the vibrational quantum numbers v and v' of the electronic initial and final states, respectively, and $D(\omega_{bv',av}-\omega)$ is the Lorentzian line shape function.

Based on the Born–Oppenheimer adiabatic approximation,

$$\varphi_{bv'} = \Phi_b(q,Q)\Theta_{bv'}(Q),\ \varphi_{av} = \Phi_a(q,Q)\Theta_{av}(Q) \quad (2a)$$

all vibrational modes are assumed to be decoupled,

$$\Theta_{bv'} = \prod_i \chi_{bv'_i}(Q_i),\ \Theta_{av} = \prod_i \chi_{av_i}(Q_i) \quad (2b)$$

and the electronic transition dipole moment $\vec{\mu}_{ba}$ can be expanded around the equilibrium geometry $Q = 0$,

$$\vec{\mu}_{ba}(Q) = \vec{\mu}_{ba}(0) + \sum_i \left(\frac{\partial\vec{\mu}_{ba}}{\partial Q_i}\right)_0 Q_i + \cdots \quad (2c)$$

the absorption coefficient for the symmetry-allowed transition is approximated as

$$\alpha(\omega) = \frac{4\pi^2\omega}{3\hbar c}|\vec{\mu}_{ba}(0)|^2 \prod_i\sum_{\nu_i}\sum_{\nu'_i} P_{av_i}|\langle\chi_{bv'_i}|\chi_{av_i}\rangle|^2 D(\omega_{bv'_i,av_i}-\omega) \quad (3)$$

while for symmetry-forbidden transition ($\vec{\mu}_{ba}(0) = 0$), the second term of eqn (2c) dominates. It follows that

$$\alpha(\omega) = \frac{4\pi^2\omega}{3\hbar c} \sum_v\sum_{v'} P_{av}\left|\sum_i\left(\frac{\partial\mu_{ba}}{\partial Q_i}\right)_0\langle\chi_{bv'_i}|Q_i|\chi_{av'_i}\rangle\prod_{j\neq i}\langle\chi_{bv'_j}|\chi_{av_j}\rangle\right|^2 \times D(\omega_{bv',av}-\omega) \quad (4)$$

The inducing mode Q_i leads to $(\partial\mu_{ba}/\partial Q_i)_0 \neq 0$, which represents a transition moment induced by a distortion away from the equilibrium geometry. The symmetry of the inducing mode is determined according to the symmetry rule. For fluorescence spectra, a form similar to eqn (4) can be obtained. The first derivatives of the transition dipole moment, $(\partial\mu_{ba}/\partial Q_i)_0 \neq 0$, can be described by the first-order perturbation theory.

Note that the electronic Hamiltonian can be expressed as

$$H_{el}(q;\{Q\}) = T_{el}(q) + V_{ee}(q) + V_{eN}(q,Q) + V_{NN}(Q) \quad (5a)$$

where $T_{el}(q)$ is the electronic kinetic operator, $V_{ee}(q)$ the electron–electron interaction energy, $V_{NN}(Q)$ the nuclear–nuclear interaction energy, and $V_{eN}(q,Q)$ the nuclear–electron interaction energy. q and Q denote the coordinates of electrons and nuclei, respectively. The electronic part of $H_{el}(q;\{Q\})$ is implicitly dependent on the nuclear coordinates. At the equilibrium geometry ($Q = 0$),

$$H^0_{el}\Phi^0_a = E(\Phi^0_a)\Phi^0_a \quad (5b)$$

$$H^0_{el}(q;\{0\}) = T_{el}(q) + V_{ee}(q) + V_{eN}(q,0) \quad (5c)$$

The electron–nuclear interaction can be expanded as

$$V_{eN}(q,Q) = V_{eN}(q,0) + \sum_i\left(\frac{\partial V_{eN}}{\partial Q_i}\right)_0 Q_i + \cdots \quad (5d)$$

By means of the first-order perturbation method, the electronic wave functions are therefore expressed as

$$\Phi_a = \Phi_a^0 + \sum_{a'} \frac{\left\langle \Phi_{a'}^0 \left| \sum_i (\partial V_{eN}/\partial Q_i)_0 Q_i \right| \Phi_a^0 \right\rangle}{E(\Phi_a^0) - E(\Phi_{a'}^0)} \Phi_{a'}^0 \qquad (6a)$$

$$\Phi_b = \Phi_b^0 + \sum_{b'} \frac{\left\langle \Phi_{b'}^0 \left| \sum_i (\partial V_{eN}/\partial Q_i)_0 Q_i \right| \Phi_b^0 \right\rangle}{E(\Phi_b^0) - E(\Phi_{b'}^0)} \Phi_{b'}^0 \qquad (6b)$$

Then the electronic transition dipole moment can be obtained as

$$\begin{aligned} \vec{\mu}_{ba}(Q) = \langle \Phi_b | \vec{\mu} | \Phi_a \rangle &= \langle \Phi_b^0 | \vec{\mu} | \Phi_a^0 \rangle \\ &+ \sum_i \left\{ \sum_{a'} \frac{\langle \Phi_{a'}^0 | (\partial V_{eN}/\partial Q_i)_0 | \Phi_a^0 \rangle}{E(\Phi_a^0) - E(\Phi_{a'}^0)} \langle \Phi_b^0 | \vec{\mu} | \Phi_{a'}^0 \rangle \right. \\ &\left. + \sum_{b'} \frac{\langle \Phi_{b'}^0 | (\partial V_{eN}/\partial Q_i)_0 | \Phi_b^0 \rangle}{E(\Phi_b^0) - E(\Phi_{b'}^0)} \langle \Phi_{b'}^0 | \vec{\mu} | \Phi_a^0 \rangle \right\} Q_i \end{aligned} \qquad (7)$$

Note that small terms are ignored in eqn (7). For symmetry forbidden transitions, $\vec{\mu}_{ba}(0) = \langle \Phi_{ba}^0 | \vec{\mu} | \Phi_a^0 \rangle = 0$, it follows that

$$\begin{aligned} \left(\frac{\partial \mu_{ba}}{\partial Q_i} \right)_0 &= \sum_{a'} \frac{\langle \Phi_{a'}^0 | (\partial V_{eN}/\partial Q_i)_0 | \Phi_a^0 \rangle}{E(\Phi_a^0) - E(\Phi_{a'}^0)} \langle \Phi_b^0 | \vec{\mu} | \Phi_{a'}^0 \rangle \\ &+ \sum_{b'} \frac{\langle \Phi_{b'}^0 | (\partial V_{eN}/\partial Q_i)_0 | \Phi_b^0 \rangle}{E(\Phi_b^0) - E(\Phi_{b'}^0)} \langle \Phi_{b'}^0 | \vec{\mu} | \Phi_a^0 \rangle \end{aligned} \qquad (8)$$

Here, $\langle \Phi_b^0 | \vec{\mu} | \Phi_{a'}^0 \rangle$ and $\langle \Phi_{b'}^0 | \vec{\mu} | \Phi_a^0 \rangle$ are symmetry-allowed transition moments; $\frac{\langle \Phi_{a'}^0 | (\partial V/\partial Q_i)_0 | \Phi_a^0 \rangle}{E(\Phi_a^0) - E(\Phi_{a'}^0)}$ and $\frac{\langle \Phi_{b'}^0 | (\partial V/\partial Q_i)_0 | \Phi_b^0 \rangle}{E(\Phi_b^0) - E(\Phi_{b'}^0)}$ are the vibronic couplings related to the electronic states Φ_a^0 and Φ_b^0.

Next, the vibrational modes are classified in order to calculate FC overlap integrals. Based on the displaced oscillator model ($\omega_i' = \omega_i$, $Q_i' = Q_i - \Delta Q_i$), $\Delta Q_i \neq 0$ for those totally symmetric modes. ΔQ_i is the displacement of the oscillator between two electronic states. In general, the inducing modes are usually non-total symmetric. For instance, only those modes of e_{2g} symmetry in benzene can induce the vibronic coupling in radiation processes between S_0 ($^1A_{1g}$) and S_1 ($^1B_{2u}$) states based on eqn (8). $\langle \chi_{bv_i'} | Q_i | \chi_{av_i} \rangle \neq 0$ requires $\nu_i' = \nu_i \pm 1$ for the inducing mode.

The remaining modes in the vibrational overlap integrals are separated into two parts, the totally symmetric (j_T) and other non-totally (j_{NT}) symmetric modes:

$$\prod_{j \neq i} \langle \chi_{bv_j'} | \chi_{av_j} \rangle = \prod_{k \in j_T} \langle \chi_{bv_k'} | \chi_{av_k} \rangle \prod_{l \in j_{NT}} \langle \chi_{bv_l'} | \chi_{av_l} \rangle \qquad (9)$$

Eqn (9) determines the profile of the spectrum. For the totally-symmetric vibrational modes, j_T, $\Delta Q_k \neq 0$, the Franck–Condon factors for each mode of this kind can be expressed as

$$|\langle \chi_{bv_k'} | \chi_{a0} \rangle|^2 = \frac{S_k^{\nu_k'}}{\nu_k'!} e^{-S_k} \qquad (10)$$

where the Huang-Rhys factor is defined as $S_k = \frac{\omega_k}{2\hbar}(\Delta Q_k)^2$. It should be noted that eqn (10) is based on the displaced oscillator approximation and is applicable only to the case of transitions $0 \leftrightarrow \nu_k'$. Each totally symmetric mode with $S_k \neq 0$ constructs a progression $k_0^{\nu_k'}(\nu_k' \leftarrow 0)$ in the spectra. The remaining modes are non-totally symmetric, j_{NT}, $\Delta Q_l = 0$, and each of these modes constructs a sequence $l_{\nu_l'}^{\nu_l'}$ ($\nu_l' \leftarrow \nu_l$, $\nu_l' = \nu_l$ or $\nu_l = \nu_l \pm 2$, *etc.*). So it is concluded that for symmetry-forbidden transitions, the absorption spectra are of $I_{\nu_i'}^{\nu_i'} K_0^{\nu_k'} L_{\nu_l'}^{\nu_l'}$, where I, K and L refer to the inducing mode, the totally-symmetric modes, and the other modes, respectively.

Parmenter *et al.*[26] reported a detailed assignment of the spectrum for the benzene 260-nm transition *via* single vibronic level fluorescence. They have assigned $6_0^1 5_0^2$, $6_0^1 11_0^2$, $6_0^1 16_0^2$ and $6_0^1 17_0^2$ peaks in the spectra. That the l_v^{v+2} peaks appear is because the distortion effect of these modes is large, and therefore the vibrational overlap integrals $\langle \chi_v | \chi_{v\pm2} \rangle$ are large. In general, the Franck–Condon factors for distorted oscillators are[31]

$$F_{\nu_l',0} = \frac{\sqrt{\omega_l \omega_l'}}{\omega_l + \omega_l'} \left(\frac{\omega_l' - \omega_l}{\omega_l + \omega_l'} \right)^{\nu_l'} \frac{\nu_l'!}{2^{\nu_l'-1}[(\nu_l'/2)!]^2} \qquad (11)$$

where ν_l' is an even integer. It is seen that unless $|\omega_l' - \omega_l|$ is large, $F_{\nu_l',0}$ is much smaller than the unity for $\nu_l' \neq 0$; in other words, the distortion effect due to the quadratic coupling is unimportant. If the frequency difference between the two electronic states is not negligible, it influences the spectrum.

In addition, when the temperature is not very low, and the molecules are in thermal equilibrium, some modes could distribute in their vibrational excited states, especially for those modes with low frequencies. Thus, some modes are initially at $\nu_i = 1,2,\ldots$, which results in the hot bands in the spectra.

It should be noted that the anharmonicity in the potential curve is neglected here. In general, the anharmonicity has two effects: to scramble the various normal modes and to cause changes in vibrational level spacing of a normal mode. The first effect is necessary in intramolecular vibrational relaxation. It is generally assumed that the vibrational relaxation time is much shorter than that of the electronic relaxation so that the transitions always originate from a Boltzmann distribution of vibrational levels. The second effect may cause changes in the Franck–Condon factor in cases where there are modifications of frequencies and coordinates. Therefore, the second effect can make a band shifted and a profile changed.[1,32,33]

Rates of IC

IC is defined as radiationless transitions between two electronic states of the same multiplicity. Its rate constants can also be obtained by the perturbation method as for the optical absorption discussed above. The perturbation Hamiltonian for IC is the Born–Oppenheimer coupling.[1] With the application of the Condon approximation, the perturbation term is further simplified. Following the same procedures as for the absorption but with different perturbation term, the rate of IC can be obtained. Note that the perturbation term for this process is time-independent. General considerations for IC have been reported.[1,34] In the present work, we are

concerned with the single level rate constants of IC based on the displaced and distorted oscillator approximations.

Considering the $T = 0$ K case, the rate constant for IC $a0_p \rightarrow b$ promoted by the promoting mode v_p is expressed, in terms of Fermi's Golden rule, as

$$W_{a0_p\rightarrow b} = \frac{1}{\hbar^2}|R_{ba}(Q_p)|^2 \int_{-\infty}^{+\infty} \mathrm{d}t e^{it(\omega_{ba}+\omega_p)} \prod_{i\neq p} G_i(t) \quad (12)$$

where

$$R_{ba}(Q_p) = \frac{\hbar\omega_p}{\sqrt{2}} \left\langle \Phi_b \left| \frac{\partial \Phi_a}{\partial Q_p} \right\rangle \right.,$$

$G_i(t) = \sum_{\nu_i'=0}^{\infty} |\langle \chi_{b\nu_i'}|\chi_{a0_i}\rangle|^2 \exp\{it[(\nu_i'+\frac{1}{2})\omega_i' - \frac{1}{2}\omega_i]\}$, ω_{ba} is the energy gap between the two electronic states, and ω_p is the frequency of the promoting mode. For a displaced oscillator, $G_i(t) = \exp[S_i(-1 + e^{it\omega_i})]$.

Similarly for a distorted oscillator, $G_i(t)$ is given by

$$G_i(t) = \frac{2\sqrt{\omega_i\omega_i'}e^{-\frac{it\omega_i}{2}}}{[(\omega_i+\omega_i')^2 e^{-it\omega_i'} - (\omega_i-\omega_i')^2 e^{it\omega_i'}]^{\frac{1}{2}}} \quad (13)$$

If the distortion effect is not large, it is approximately

$$G_i(t) = \frac{2\sqrt{\omega_i\omega_i'}}{(\omega_i+\omega_i')} e^{\frac{it}{2}(\omega_i'-\omega_i)} \quad (14)$$

Eqn (12) can be rewritten as

$$G_i(t) = g_i(t) e^{\frac{it}{2}(\omega_i'-\omega_i)} \quad (15)$$

where

$$g_i(t) = \frac{2\sqrt{\omega_i\omega_i'}}{(\omega_i+\omega_i')\left[1 - \frac{(\omega_i-\omega_i')^2}{(\omega_i+\omega_i')^2} e^{2it\omega_i'}\right]^{\frac{1}{2}}} \quad (16)$$

From eqn (16), it can be seen that $g_i(t) = 1$ if the mode has little distortion ($\omega_i' \approx \omega_i$), and therefore $G_i(t) = 1$. That means these oscillators would not affect the rate constants of IC. Thus if there is only one distortion mode $g_d(t)$, then

$$W_{a0_p\rightarrow b} = \frac{1}{\hbar^2}|R_{ba}(Q_p)|^2 \int_{-\infty}^{+\infty} \mathrm{d}t \cdot g_d(t) \exp\left[it\left(\omega_{ba}+\omega_p+\frac{\omega_d'-\omega_d}{2}\right) + \sum_i S_i(-1+e^{it\omega_i})\right] \quad (17)$$

while for the case with multiple distorted modes, it has the general form of

$$W_{a0_p\rightarrow b} = \frac{1}{\hbar^2}|R_{ba}(Q_p)|^2 \int_{-\infty}^{+\infty} dt \exp\left[it\left(\omega_{ba}+\omega_p+\sum_d \frac{\omega_d'-\omega_d}{2}\right) + \sum_i S_i(-1+e^{it\omega_i})\right] \prod_d g_d(t) \quad (18)$$

By using the saddle-point method, we obtain

$$W_{a0_p\rightarrow b} = \frac{1}{\hbar^2}|R_{ba}(Q_p)|^2 \prod_d g_d(t^*) \sqrt{\frac{2\pi}{\sum_i S_i\omega_i^2 e^{it^*\omega_i}}} \times \exp\left[it^*\left(\omega_{ba}+\omega_p+\sum_d \frac{\omega_d'-\omega_d}{2}\right) + \sum_i S_i(-1+e^{it^*\omega_i})\right] \quad (19)$$

where t^*, the saddle-point value, is determined by

$$\omega_{ab} - \omega_p - \sum_d \frac{\omega_d'-\omega_d}{2} = \sum_i S_i\omega_i e^{it^*\omega_i} \quad (20)$$

$\prod_d g_d(t)$ is also estimated by $\prod_d g_d(t^*)$. Though $g_d(t)$ is close to 1 for each distorted mode, the multiplication of all the distorted modes would affect the rate constants to some extent.

Results and discussion

Properties of the ground and excited states of benzene

Ab initio and DFT (density functional theory) calculations were performed with Ganssian 03[35] and MOLPRO[36] packages. The stable geometry of benzene in its ground electronic state (S_0 $^1A_{1g}$) was determined at various levels including HF (Hartree–Fock, HF results were not presented), MP2 (second order Møller–Plesset perturbation theory), DFT, and CASSCF (complete active space self-consistent field). The selection of the basis sets should be careful, for some special basis sets at MP2 level give imaginary frequencies for the out-of-plane vibrational modes of benzene.[37] Most calculations in the present work were performed with the basis set 6-31+G(d,p), and also a few basis sets, *e.g.* cc-pVTZ (correlation consistent polarized valence triple-zeta basis set) and aug-cc-pVTZ (augmented correlation consistent polarized valence triple-zeta), were selected to verify that the calculation was not sensitive to basis sets. For the lowest excited state (S_1 $^1B_{2u}$) of benzene, its stable structures were determined at the CASSCF(6,6)/6-31+G(d,p) level. The active space for the CASSCF calculations was composed of 6 active π electrons distributed in 6 active orbitals ($1a_{2u}$ + $2e_{1g}$ + $2e_{2u}$ + $1b_{2g}$ within the D_{6h} symmetry, or $2b_{1u}$ + $1b_{2g}$ + $2b_{3g}$ + $1a_u$ within the D_{2h} symmetry, or $3a_u$ + $3b_g$ within the C_{2h} symmetry) formed by the linear combination of carbon $2p_z$ atomic orbitals. Although larger active space which allows for the treatment of the Rydberg excited states[38,39] would yield more accurate results, this smaller (6,6) one has been proven able to describe the potential energy surfaces well and is preferred due to its low cost.[3] The CIS results were also given though they are clearly unreliable.[5] The potential energy surfaces by the CASSCF method were used for subsequent calculations of spectrum simulation and rate constants of the IC.

The geometries of the two states of benzene were fully optimized within the D_{6h} symmetry. Its stable geometries are listed in Table 1. The optimization methods for the ground state included MP2 (FC), B3LYP, and CASSCF(6,6).

Table 1 Bond distances (Å) for the ground and excited states

		R_{CC}	R_{CH}
S_0	Expt.[a]	1.396	1.083
	MP2(FC)/6-31+G(d,p)	1.399	1.083
	B3LYP/6-31+G(d,p)	1.398	1.086
	CAS(6,6)/6-31+G(d,p)	1.398	1.076
	CASPT2[a]	1.396	1.081
S_1	Expt.[a]	1.432	1.084
	CIS/6-31+G(d,p)	1.415	1.074
	TD-B3LYP/6-31+G(d,p)	1.428	1.084
	CAS(6,6)/6-31+G(d,p)	1.435	1.074
	CASPT2[a]	1.432	1.080

[a] Ref. 3 and references cited therein.

All these methods gave the correct D_{6h} symmetry. Compared with the observations, CASSCF gave a little longer CC bond lengths for this method did not account for the dynamic correlation, and gave too short CH bond lengths for the chosen active space did not include the σ orbitals. On the other hand, as shown in Table 1, the geometries calculated by MP2 and B3LYP were almost the same as the experimental observations.

For the excited state, CIS, TD-B3LYP and CASSCF (6,6) were employed. The results suggested that CIS is not recommended, while the TD (time-dependent)-DFT method is not only low-cost but also reliable.[5] The CASSCF geometries agreed well with the experimental observations and were used for the subsequent calculations. Based on the CASSCF wave functions as a zeroth-order approximation and adding a second-order perturbation, the CASPT2 results were even closer to the experimental observations, but also much more computationally expensive.

Table 2 lists the calculated and experimental harmonic frequencies for the two states. For the ground state MP2 and B3LYP the results were very close to the observations, while CASSCF was a little worse than the other two methods.

Table 3 Vertical and adiabatic excitation energies (eV)

	Vertical	Adiabatic
Expt.[a]	4.90	4.72
CIS/6-31+G(d,p)	6.06	5.92[b]
CAS(6,6)/6-31+G(d,p)	4.96	4.76[c]
TD-B3LYP/6-31+G(d,p)	5.38	5.13[b]
CASPT2[a]	4.68	4.37

[a] Ref. 3 and references cited therein. [b] Without ZPVE (zero point vibrational energy). [c] Without ZPVE, or 4.61 eV with ZPVE.

The electronic excitation energies, including vertical and adiabatic excitation energies, are given in Table 3. In comparison with the experimental observations, different theoretical calculations overestimated or underestimated the energies. CIS and TD-DFT results were pretty higher than the experiment measurement, while CASPT2 results were lower. The CASSCF results were the best among them and were used in the subsequent calculations.

Vibronic coupling

For symmetry-forbidden transitions, the fact that the vibronic peaks can show up in one-photon absorption spectra is due to the vibronic coupling—it can borrow intensities from symmetry-allowed transitions to intermediate states through the inducing mode. Since the intensity of vibronic coupling is inversely-proportional to the energy differences between two states, only the states close in energy can be coupled efficiently. For benzene's first excited state, $^1A_{1g}$–$^1B_{2u}$ transition is symmetry-forbidden, but it can borrow intensities from the allowed transitions $^1A_{1g}$–$^1E_{1u}$ and $^1B_{2u}$–$^1E_{2g}$. Ignoring the terms of higher coupling states which have larger energy differences, it follows that

$$\left(\frac{\partial\vec{\mu}_{ba}}{\partial Q_i}\right)_0 = \sum_{b'} \frac{\langle\Phi^0_{b'}|(\partial V/\partial Q_i)_0|\Phi^0_b\rangle}{E(\Phi^0_b) - E(\Phi^0_{b'})}\langle\Phi^0_a|\vec{\mu}|\Phi^0_{b'}\rangle \qquad (21)$$

Table 2 Vibrational frequencies (cm^{-1}) of the ground and excited states

		S_0				S_1		
Modes[a]	Sym	Expt.[b]	MP2(FC)	B3LYP	CAS(6,6)	Expt.[b]	CIS	CAS
1	A_{1g}	993	1019	1012	1036	923	1026	965
2	A_{1g}	3074	3277	3208	3368	3093	3404	3391
3	a_{2g}	1350	1391	1377	1491	1327	1481	1466
4	b_{2g}	707	214	712	729	365	397	495
5	b_{2g}	990	879	1012	1039	745	914	721
6	e_{2g}	608	615	619	652	521	571	579
7	e_{2g}	3057	3252	3182	3339	3077	3376	3363
8	e_{2g}	1600	1662	1641	1729	1516	1716	1662
9	e_{2g}	1178	1218	1198	1267	1148	1266	1240
10	e_{1g}	847	837	861	875	581	728	607
11	a_{2u}	674	675	686	711	515	652	538
12	b_{1u}	1010	1014	1017	1097		1083	1066
13	b_{1u}	3057	3242	3173	3329		3369	3356
14	B_{2u}	1310	1465	1353	1337	1570	1835	1835
15	B_{2u}	1149	1195	1176	1181	1150	1272	1258
16	e_{2u}	399	376	411	431	238	241	292
17	e_{2u}	967	897	982	1000	717	884	686
18	e_{1u}	1038	1074	1061	1107	920	1067	963
19	e_{1u}	1484	1530	1515	1618	1405	1584	1539
20	e_{1u}	3065	3268	3198	3357	3084	3392	3378

[a] Wilson numbering, ref. 40. [b] Ref. 3 and literatures cited in that paper.

Table 4 Vibronic coupling between various states of benzene in C_{2h} symmetry

	$\langle\Phi^0_{b'}(b'=3^1B_u)\|(\partial V/\partial Q_i)_0\|\Phi^0_b\rangle$	$\langle\Phi^0_{b'}(b'=4^1B_u)\|(\partial V/\partial Q_i)_0\|\Phi^0_b\rangle$
$^1Q_6$	0.00174	−0.02494
$^2Q_6$	0.02355	0.01261
$^1Q_7$	−0.00458	−0.00281
$^2Q_7$	−0.00034	0.00485
$^1Q_8$	−0.00010	0.00307
$^2Q_8$	−0.00201	−0.00839
$^1Q_9$	−3.9E-05	0.00132
$^2Q_9$	−0.00082	−0.00392

with $a = {}^1A_{1g}$, $b = {}^1B_{2u}$, $b' = {}^1E_{1u}$. NACME (non-adiabatic coupling matrix elements) with respect to Cartesian coordinates were calculated directly by SA-MCSCF (state-averaged multi-configuration self-consistent field) at the equilibrium geometry of the ground state, and then were transformed to those with respect to the dimensionless normal mode vectors. According to the correlation table, the symmetry of benzene was lowered to C_{2h} (with the z-axis as the principal C_2 axis) for the practical calculations by SA-MCSCF. In the C_{2h} symmetry, the electronic states denoted in eqn (21) were assigned as $a = 1^1A_g$, $b = 1^1B_u$, $b' = 3^1B_u$ and 4^1B_u. Table 4 lists the calculation of the vibronic couplings along each inducing mode in the C_{2h} symmetry. Note that the inducing modes in the D_{6h} symmetry are of the doubly degenerated e_{2g} irreducible representation. The transition dipole moments to the intermediate states were $\langle\Phi^0_a|\mu|\Phi^0_{b'}(b'=3^1B_u)\rangle = -0.17240\vec{i} - 2.23992\vec{j}$ and $\langle\Phi^0_a|\mu|\Phi^0_{b'}(b'=4^1B_u)\rangle = 2.23992\vec{i} - 0.17240\vec{j}$ in a.u. unit. Using these quantities, the intensities of transitions were obtained. Table 5 gives the relative intensities normalized with respect to 6^1_0. The present relative intensities of false origins 9^1_0 and 7^1_0 seemed quite reasonable. The origin 8^1_0 seemed to be overestimated, compared with the experimental observations and CAS investigations. However, previous CIS results for this origin were consistent with the present results. The allowed transition dipole moments were generally reliable. The values of the energy of the electronic state were essential for the absolute intensities; however, it cancelled out for the doubly degenerate $^1E_{1u}$ state. Therefore the discrepancies would be resulted from the accuracy of SA-MCSCF, or it required more critical convergence criteria as suggested by J. Werner.[41]

Spectrum simulation

As derived in the Theory section, the spectra of the $^1A_{1g}$–$^1B_{2u}$ transition are of $I^{v'_i}_{v_i}K^{v'_k}_0L^{v'_l}_{v_l}$. At $T = 0$ K, or the temperature that is low enough to let all $\nu_i = 0$, it follows that: (a) The inducing modes can be excited only with $v'_i = 1 \leftarrow v_i = 0$ in I^1_0 ($I = \nu_6,\nu_7,\nu_8,\nu_9$). These modes are of the e_{2g} irreducible representation. (b) The totally symmetric vibrational modes can be excited with $v'_k = 0, 1, 2, \cdots \leftarrow v_k = 0$ in $K^{v'_k}_0$ ($K = \nu_1, \nu_2$). These modes are of the a_{1g} irreducible representation. (c) The other modes can be excited only $v'_l = 0 \leftarrow v_l = 0$ based on the distorted oscillator model or $v'_l = 0, 2, 4, \cdots \leftarrow v_l = 0$ if the distortion effect is not negligible. Then eqn (4) is explicitly rewritten as

$$\alpha(\omega) = \frac{4\pi^2\omega}{3\hbar c}\sum_{v'}\left|\sum_i\left(\frac{\partial\mu_{ba}}{\partial Q_i}\right)_0\right|^2 I^1_0K^{v'_k}_0L^{v'_l}_0D(\omega_{bv',a0}-\omega) \tag{22}$$

$$I^1_0 = |\langle\chi_{b1}|Q_i|\chi_{a0}\rangle|^2 \tag{23a}$$

$$K^{v'_k}_0 = \left|\prod_{k\in j_T}\langle\chi_{bv'_k}|\chi_{a0}\rangle\right|^2 \tag{23b}$$

$$L^{v'_l}_0 = \left|\prod_{l\in j_{NT}}\langle\chi_{bv'_l}|\chi_{a0}\rangle\right|^2 \tag{23c}$$

So the spectra possess four false origins by promoting modes ν_6, ν_7, ν_8 and ν_9. The progressions of the totally symmetric modes ν_1 and ν_2 are the main bands.

The peaks induced by the ν_6 mode were firstly simulated at $T = 0$ K. Other peaks by ν_6, ν_7, ν_8 and ν_9 were simulated similarly but with much smaller vibronic couplings and different locations. The Huang-Rhys factors of the two totally symmetric modes, ν_1 and ν_2, were $S_1 = 1.6507$ and $S_2 = 0.0090$, respectively. Therefore, the spectrum showed the major progressions of $6^1_0 1^{v'_1}_0$ only if other effects were neglected.

As mentioned above, the spectra of the weak symmetry-forbidden transition are distinguishable, and many more peaks have been assigned experimentally. Therefore, more effects should be considered in the simulation. The distorted corrections are generally not important, which makes the spectrum profile mainly of the progression $6^1_0 1^{v'_1}_0$ based on the displaced oscillator model ($T = 0$ K). However, these corrections should be included, especially for those modes with greatly shifted frequencies. From eqn (11), it follows that

$$F_{b0',a0} = \frac{2\sqrt{\omega\omega'}}{\omega+\omega'} \tag{24}$$

Table 6 gives the distortion effects of these modes. Although the effects (if only 0–0′ transitions occur in these modes) would not change the relative intensities of the spectrum, they could somewhat lower the absolute intensities.

For $T \neq 0$ K, some modes could distribute in their vibrationally excited states, especially for those modes with low frequencies. Then, at the initial state, some modes can exist with their vibrational quantum number $v_i = 1, 2, \ldots$ Thus hot bands can be observed in the spectrum. Based on the Boltzmann distribution rule, $N_i/N_0 = e^{-(\xi_i-\xi_0)/k_BT}$, and the harmonic oscillator approximation, $\xi_{v_i} = (\nu_i + 1/2)\hbar\omega_i$, it gives that $N_{v_i}/N_0 = e^{-\nu_i\hbar\omega_i/k_BT}$. At $T = 300$ K, the vibrational distributions of those modes with low frequencies are listed in Table 7. It is seen that excitations of the ν_{16} mode lead to an

Table 5 Relative intensities of the vibronically induced e_{2g} false origins

Lines	Expt.[a]	Expt.[a]	Present work	CIS[a]	CAS[a]
6^1_0	100.0	100.0	100.0	100.0	100.0
7^1_0	3.6	5.9	4.2	3.0	5.8
8^1_0	0.6	—	6.4	5.8	0.4
9^1_0	1.8	2.3	1.4	0.3	4.0

[a] Ref. 3 and references cited therein.

Table 6 Distortion effects

Mode	4	5	10	11	14	16	17	18
S_0 state freq./cm^{-1}	729	1039	875	711	1337	431	1000	1107
S_1 state freq./cm^{-1}	495	721	607	538	1835	292	686	963
Freq. shift/cm^{-1}	−234	−318	−268	−173	498	−139	−314	−144
$F_{b0',a0}$	0.9817	0.9835	0.9835	0.9903	0.9876	0.9814	0.9825	0.9976
$F_{b2',a0}$	0.0178	0.0160	0.0161	0.0096	0.0122	0.0180	0.0170	0.0024

Table 7 The vibrational distribution of modes with low frequencies (<1000 cm^{-1}) at T = 300 K

Mode	4	6	10	11	16	17
S_0 state freq./cm^{-1}	729	652	875	711	431	1000
N_1/N_0	0.0303	0.0438	0.0150	0.0329	0.1265	0.0082
N_2/N_0	0.0010	0.0020	0.0000	0.0010	0.0160	0.0000

intense hot band from the e_{2g} modes. The same behavior was observed in earlier investigations.[3] Hence, there will be some sequences $1' \leftarrow 1$ of the modes ν_4, ν_{10}, ν_{11}, ν_{16}, and ν_{17}.

Thus, the hot bands associated with 6_0^1 were constructed including two progressions and five sequences, $6_0^1 K_0^{\nu_k} L_1^{1_l}$; where $K = \nu_1,\nu_2$ and $L = \nu_4,\nu_{10},\nu_{11},\nu_{16},\nu_{17}$, based on the displaced oscillator model. Their combinations such as $6_0^1 1_0^{\nu_1'} 16_1^1$ could also be observed. If the distortion effect was considered, $6_0^1 L_0^{2'}$ could also appear. Similarly, the hot bands of 6_1^0 and 6_1^2 were constructed, but special care should be taken. According to the relation

$$\langle \chi_n|Q|\chi_m\rangle = \sqrt{\frac{n+1}{2\beta}}\delta_{m,n+1} + \sqrt{\frac{n}{2\beta}}\delta_{m,n-1},$$

it gives the ratios of intensities of these origins $6_0^1 : 6_1^0 : 6_1^2$ = 1 : 1 : 2. Other peaks induced by modes ν_7, ν_8 and ν_9 can be constructed in a similar way.

In summary, the peaks in the simulated spectrum include: $6_0^1 1_0^n$, $6_0^1 1_0^n 2_0^1$, $6_0^1 X_1^1$(X = 4,10,11,16,17), $6_0^1 16_2^2$, $6_0^1 1_0^1 X_1^1$, $6_0^1 1_0^1 16_2^2$, $6_0^1 1_0^2 X_1^1$, $6_0^1 1_0^2 16_2^2$, $6_0^1 1_0^3 X_1^1$, $6_0^1 1_0^3 16_2^2$, $6_0^1 1_0^4 16_1^1$, $6_0^1 1_0^5 16_1^1$, $6_0^1 Y_0^2$(Y = 4, 5, 10, 11, 14, 16, 17), $6_0^1 1_0^1 Y_0^2$, $6_0^1 1_0^2 Y_0^2$, $6_0^1 1_0^3 Y_0^2$, $6_1^0 1_0^n$, $6_1^2 1_0^n$, $7_0^1 1_0^n$, $8_0^1 1_0^n$, $9_0^1 1_0^n$. In other words, the spectrum was simulated peak by peak at 300 K, as shown in Fig. 1. The experimental spectrum in Fig. 1 is adopted from ref. 39. The present CASSCF results calculated above were utilized in the simulation of the symmetry-forbidden transition. No *ab initio* result was scaled to approach the observations. The dephasing or damping constant in the Lorentzian function was set as 0.001 eV in absorption. Owing to the symmetry, the transition dipole moment vanishes and the 0–0′ peak could not be observed in the spectra. The main peaks are the progression from the totally symmetric mode ν_1, whose Huang-Rhys factor is 1.6507, induced by the promoting mode ν_6. Though it was reported that the inclusion of Duschinsky effect may raise the intensities for the transitions by 20%,[42] our simulated spectra without considering this effect did show good agreement with the experiment results.[43] Notably, the present CASSCF spectrum gave a longer progression of ν_1 mode than the observations. Similar investigations can also be found in ref. 3. In addition, the calculated peaks by non-total symmetric

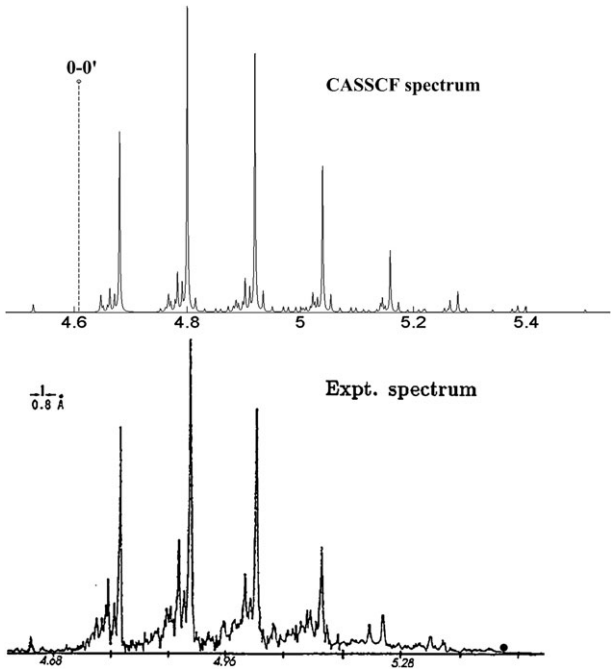

Fig. 1 Spectrum for the absorption $1^1A_{1g} \rightarrow 1^1B_{2u}$ in benzene (x in eV, y in arbitrary units).

modes seem underestimated. It is because that calculated frequencies are generally overestimated by CASSCF. Thus the vibrational distributions of these modes are underestimated according to the Boltzmann distribution rule and FC factors are underestimated according to eqn (24). Besides, the anharmonicities are also important in calculating FC factors.[44] Note, the present simulation only took the first order vibronically induced transitions into account, while the higher order corrections and some other effects may influence the spectrum,[45] and surely the calculations can be more expensive. Without these effects, the major progressions as well as the weak peaks, hot bands and so on are all in good agreement with the experimental observations. Similarly, the fluorescence spectrum for $1^1A_{1g} \leftarrow 1^1B_{2u}$ can be simulated as shown in Fig. 2, with Huang-Rhys factors S_1 = 1.5384, S_2 = 0.0095. The fluorescence spectra are also consistent with the experimental observations of ref. 20. The damping constant was set as 0.004 eV in the fluorescence.

Rate constants of IC

The formalism described in the Theory section allows the calculation of the rate constants of IC between various singlet

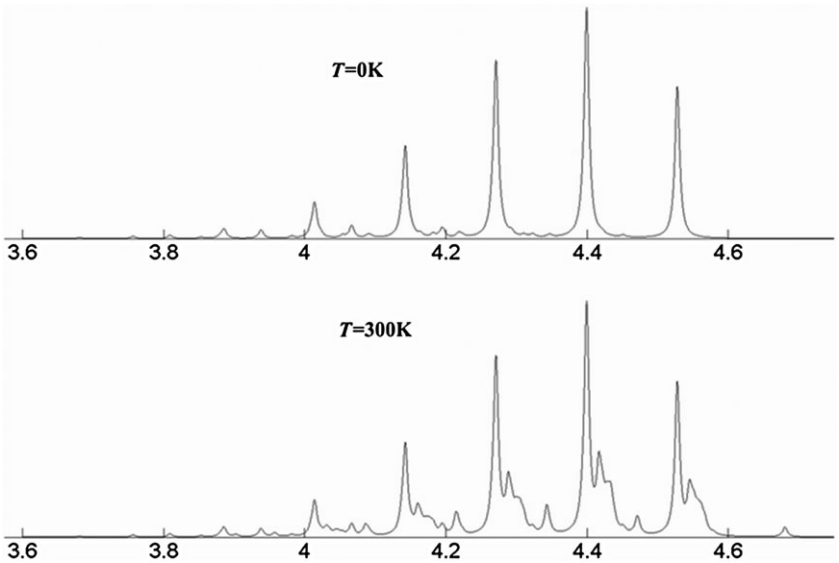

Fig. 2 Spectrum for the fluorescence $1^1A_{1g} \leftarrow 1^1B_{2u}$ in benzene (x in eV, y in arbitrary units).

electronic states using vibronic coupling. It can be easily shown that

$$\left\langle \Phi_b \left| \frac{\partial \Phi_a}{\partial Q_p} \right\rangle = \frac{\langle \Phi_b^0 | (\partial V / \partial Q_p)_0 | \Phi_a^0 \rangle}{E(\Phi_a^0) - E(\Phi_b^0)} \right. \qquad (25)$$

Note that the normal coordinate Q_p is dimensionless, which makes $\langle \Phi_b | \partial / \partial Q_p | \Phi_a \rangle$ dimensionless. The single level rate constant of the IC $1^1A_{1g} \leftarrow 1^1B_{2u}$ in benzene is determined, as following eqn (19) by using the factors: energy gap between the two electronic states ω_{ba} ($\omega_{ba} < 0$); frequency of the promoting mode ω_p; Huang-Rhys factors S_i and frequencies ω_i of the totally symmetric displaced accepting modes; frequencies ω_d and ω'_d of the non-totally symmetric distorted oscillator modes; and vibronic coupling.

The promoting mode for IC $1^1A_{1g} \leftarrow 1^1B_{2u}$ is of the b_{2u} irreducible representation in terms of the symmetry rule, therefore only ν_{14} and ν_{15} modes could be promoting modes. Here we adopted $S_k = \frac{\mu_k \omega_k}{2\hbar} d_k^2$, where μ_k is the reduced mass of the mode and d_k is the difference of the Cartesian coordinates between the two states. Explicitly, S_k = Con. $\times$ $\mu_k \upsilon_k d_k^2$ with μ_k in atomic mass units, υ_k in cm^{-1}, d_k in Å, and Con. = 0.014830 (units), which makes S_k dimensionless. By this method, the Huang-Rhys factors are S_1 = 1.4615, S_2 = 0.3241, respectively. The vibronic couplings were calculated by SA-MCSCF in the C_s symmetry. The saddle-point value it^* was numerically determined by eqn (20). Along with the energy gap ω_{ab} = 37174 $\times$ 2π cm^{-1} and the frequencies listed in Table 2, the rate constants of IC were then obtained. Table 8 lists the details of the calculation results. It is emphasized that the distortion effect of the normal modes is taken into account as described in eqn (19). This effect increases the rate constants of IC by a factor of about 2–3 in this work (Table 8).

Table 8 Calculations of the rates of IC $1^1A_{1g} \leftarrow 1^1B_{2u}$

	Q_{14}	Q_{15}
$it^*(cm/2\pi)$	9.78×10^{-4}	9.85×10^{-4}
$\langle \Phi_b \vert \partial / \partial Q_p \vert \Phi_a \rangle$	0.2843	−0.4042
$\prod_d g_d(t^*)$	2.2261	2.7012
W/s^{-1}	2.85×10^3	1.91×10^3

The calculated rate constants of IC induced by Q_{14} and Q_{15} are close to each other, though, both of them might be underestimated in the present work. It is due to the large energy gap between the two states and small Huang-Rhys factors and vibronic coupling. In fact, the coupling between states with a large energy difference is small. Besides, calculations of the electronic structures are essential for the understanding of IC. The general formalisms,[1] more complicated, are not employed in the work. The small rate constants show that the IC $1^1A_{1g} \leftarrow 1^1B_{2u}$ is not the main channel of the electronic relaxation. The calculated rate constants with distortion effect considered for this IC process are within the order of 10^3 s^{-1}.

The vibrational excitation is essential for the competition between various types of nonradiative decay. At very low vibrational regions of S_1 (1^1B_{2u}) state, the intersystem crossing (one of the nonradiative decay, the so-called "channel 2") might be the only nonradiative channel to decay.[29,46] Our calculated scheme for the IC described above starts from the vibrationless excited state, *i.e.*, all vibrational modes are at $v = 0$. Under these conditions, the present rate constants of IC are only about 10^{-4} of the total nonradiative rate constants (11.2×10^6 s^{-1}, see ref. 17 and 29 and references cited therein) is reasonable. The present rate constants are about 100 times larger than the previous calculated value[47] 32.4 s^{-1}. In the present work, NACME was obtained at the equilibrium geometry of the ground state 1^1A_{1g}. This approach may introduce errors because NACME can be quite large in canonical intersections.[28] Some other effects can also affect the nonradiative decay rates. The non-Condon effect might increase the IC rate constants by a factor of about 2–3.[48] In addition, an important factor involved in the anharmonic effect is the vibrational mode mixing which will increase the number of modes participated in accepting the electronic

energy involved in IC.[49] This will increase the rate of internal conversion. For this IC, the rate constants increase drastically when the excess energy above the origin of S_1 state approaches[50] 3000 cm^{-1}. In such cases, the contribution of the so-called "channel 3" (or chemical relaxation[29]) might be the major part. Also, the excitation of CH modes is more efficient for disposing of the excess energy than the higher excitation of other low-frequency modes,[51] and thus the anharmonicity of these modes can play a major part in the transfer.[52] In fact, all effects can be included if more reliable potential surfaces were obtained. Nonetheless, the present work might give an estimate of the lower limit of the rate constants of this IC, which is about 4.8×10^3 s^{-1} by summing up the contributions from the two inducing modes.

Conclusions

Transition processes can be described by the time-dependent perturbation method using the total Hamiltonian which consists of two parts: zeroth-order Hamiltonian which represents the stationary properties, and the perturbation part which accounts for the process under consideration. The two processes, symmetry-forbidden absorption/fluorescence and IC, all involving the vibronic coupling, were formulated and a practical application was reported in this work. The vibronic coupling, essential in these processes, was calculated in terms of the Herzberg–Teller expansion theory within the Born Oppenheimer approximation. For the symmetry-forbidden absorption/fluorescence, formalisms derived here took into account the temperature effect and the distortion effect, but neglected the Duschinsky effect. For the IC, the formalisms of the single level rate constant including the distortion effect were presented.

The *ab initio* calculation results for benzene, including geometries, energies, harmonic frequencies, and the symmetry, were all in good agreement with the observations and calculations in the literature. This provided the subsequent calculations, especially the spectra simulation, a reliable basis. The symmetry-forbidden absorption, $1^1A_{1g} \rightarrow 1^1B_{2u}$ in benzene, could borrow intensities through the inducing modes of the e_{2g} symmetry by vibronic coupling. The false origin induced by ν_6 mode was found the most intense due to the vibronic couplings along these normal coordinates (doubly degenerated) being large. Then the spectra for this forbidden absorption, with the distortion effect considered, were simulated peak by peak and agreed well with observations. The simulated fluorescence spectra were also consistent with the observations. The IC $1^1A_{1g} \leftarrow 1^1B_{2u}$ could be induced by promoting modes, ν_{14} and ν_{15} of the b_{2u} symmetry. Following the similar calculation method for vibronic coupling, the rate constants for this IC were obtained within the order of 10^3 s^{-1}, with the distortion effect increasing the IC by a factor of about 2–3. The present results, about 4.8×10^3 s^{-1}, might be the lower limit for the rate constants of this IC.

In conclusion, formalisms for symmetry-forbidden transitions and IC are presented based on the displaced and distorted oscillator approximations. The temperature effect and the distortion effect are taken into account for the symmetry-forbidden absorption/fluorescence. The method is ready for other applications and can be easily improved. The single level rate constant for IC includes the distortion effect and the formalisms for IC eqn (19), can be a good estimate if the potential energy surfaces are reliable. The application of the approach to benzene seems satisfactory.

Acknowledgements

This work is supported by the National Natural Science Foundation of China (No. 20873087) and the National Science Council (Taiwan). C.Z. would like to thank for support from National Science Council of the Republic of China (No. 97-2113-M-009-010-MY3). J.L. is grateful for support from National Chiao Tung University.

References

1 S. H. Lin, *J. Chem. Phys.*, 1966, **44**, 3759–3766.
2 G. Herzberg and E. Teller, *Z. Phys. Chem. B*, 1933, **21**, 410.
3 A. Bernhardsson, N. Forsberg, P. Malmqvist and B. O. Roos, *J. Chem. Phys.*, 2000, **112**, 2798–2809.
4 I. Borges Jr., A. J. C. Varandas, A. B. Rochab and C. E. Bielschowsky, *THEOCHEM*, 2003, **621**, 99–105.
5 L. Serrano-Andres and M. Merchán, *THEOCHEM*, 2005, **729**, 99–108.
6 S. H. Lin and R. Bersohn, *J. Chem. Phys.*, 1968, **48**, 2732–2736.
7 S. H. Lin, *J. Chem. Phys.*, 1970, **53**, 3766–3767.
8 S. H. Lin, *J. Chem. Phys.*, 1967, **46**, 279–282.
9 W. Siebrand, *J. Chem. Phys.*, 1967, **46**, 440–447.
10 M. Bixon and J. Jortner, *J. Chem. Phys.*, 1968, **48**, 715–726.
11 J. H. Callomon, T. M. Dunn and I. M. Mills, *Philos. Trans. R. Soc. London, Ser. A*, 1966, **259**, 499–532.
12 J. P. Doering, *J. Chem. Phys.*, 1969, **51**, 2866–2870.
13 B. Katz, M. Brith, B. Sharf and J. Jortner, *J. Chem. Phys.*, 1970, **52**, 88–102.
14 C. S. Parmenter and M. W. Schuyler, *J. Chem. Phys.*, 1970, **52**, 5366–5374.
15 H. F. Kemper and M. Stockburger, *J. Chem. Phys.*, 1970, **53**, 268–275.
16 B. K. Selinger and W. R. Ware, *J. Chem. Phys.*, 1970, **53**, 3160–3168.
17 K. G. Spears and S. A. Rice, *J. Chem. Phys.*, 1971, **55**, 5561–5581.
18 T. Inagaki, *J. Chem. Phys.*, 1972, **57**, 2526–2530.
19 T. R. Faulkner and F. S. Richardson, *J. Chem. Phys.*, 1979, **70**, 1201–1213.
20 T. W. Scott, K. S. Haber and A. C. Albrecht, *J. Chem. Phys.*, 1983, **78**, 150–157.
21 J. R. Cable and A. C. Albrecht, *J. Chem. Phys.*, 1986, **85**, 3155–3164.
22 A. Hiraya and K. Shobatake, *J. Chem. Phys.*, 1991, **94**, 7700–7706.
23 G. Oriandi, P. Palmieri, R. Tarroni, F. Zerbetto and M. Z. Zaierski, *J. Chem. Phys.*, 1994, **100**, 2458–2464.
24 G. H. Atkinsonlb and C. S. Parmenter, *J. Phys. Chem.*, 1971, **75**, 1564–1572.
25 G. H. Atkinson, C. S. Parrnenter and M. W. Schuyler, *J. Phys. Chem.*, 1971, **75**, 2336–1584.
26 A. E. W. Knight, C. S. Parmenter and M. W. Schuyler, *J. Am. Chem. Soc.*, 1975, **97**, 2005–2013.
27 R. Berger, C. Fischer and M. Klessinger, *J. Phys. Chem. A*, 1998, **102**, 7157–7167.
28 G. A. Worth, *J. Photochem. Photobiol., A*, 2007, **190**, 190–199.
29 C. S. Parmenter, *Adv. Chem. Phys.*, 1972, **22**, 365–421.
30 Y. J. Shiu, M. Hayashi, A. M. Mebel, Y.-T. Chen and S. H. Lin, *J. Chem. Phys.*, 2001, **115**, 4080–4094.
31 R.-X. He, C.-Y. Zhu, C.-H. Chin and H. S. Lin, *Sci. China Chem.*, 2008, **51**, 1166–1173.
32 H. Wang, C.-Y. Zhu, J.-G. Yu and S. H. Lin, *J. Phys. Chem. A*, 2009, **113**, 14407–14414.
33 C.-Y. Zhu, K.-K. Liang, M. Hayashi and S. H. Lin, *Chem. Phys.*, 2009, **358**, 137–146.

34 A. M. Mebel, M. Hayashi, K. K. Liang and S. H. Lin, *J. Phys. Chem. A*, 1999, **103**, 10674–10690.

35 M. J. Frisch, G. W. Trucks, H. B. Schlegel, G. E. Scuseria, M. A. Robb, J. R. Cheeseman, J. A. Montgomery, Jr., T. Vreven, K. N. Kudin, J. C. Burant, J. M. Millam, S. S. Iyengar, J. Tomasi, V. Barone, B. Mennucci, M. Cossi, G. Scalmani, N. Rega, G. A. Petersson, H. Nakatsuji, M. Hada, M. Ehara, K. Toyota, R. Fukuda, J. Hasegawa, M. Ishida, T. Nakajima, Y. Honda, O. Kitao, H. Nakai, M. Klene, X. Li, J. E. Knox, H. P. Hratchian, J. B. Cross, V. Bakken, C. Adamo, J. Jaramillo, R. Gomperts, R. E. Stratmann, O. Yazyev, A. J. Austin, R. Cammi, C. Pomelli, J. W. Ochterski, P. Y. Ayala, K. Morokuma, G. A. Voth, P. Salvador, J. J. Dannenberg, V. G. Zakrzewski, S. Dapprich, A. D. Daniels, M. C. Strain, O. Farkas, D. K. Malick, A. D. Rabuck, K. Raghavachari, J. B. Foresman, J. V. Ortiz, Q. Cui, A. G. Baboul, S. Clifford, J. Cioslowski, B. B. Stefanov, G. Liu, A. Liashenko, P. Piskorz, I. Komaromi, R. L. Martin, D. J. Fox, T. Keith, M. A. Al-Laham, C. Y. Peng, A. Nanayakkara, M. Challacombe, P. M. W. Gill, B. Johnson, W. Chen, M. W. Wong, C. Gonzalez and J. A. Pople, *GAUSSIAN 03 (Revision E.01)*, Gaussian, Inc., Wallingford, CT, 2004.

36 H.-J. Werner, P. J. Knowles, R. Lindh, F. R. Manby, M. Schütz and others, *MOLPRO, version 2009.1, a package of ab initio programs*, see http://www.molpro.net.

37 D. Moran, A. C. Simmonett, F. E. Leach III, W. D. Allen, P. v. R. Schleyer and H. F. Schaefer III, *J. Am. Chem. Soc.*, 2006, **128**, 9342–9343.

38 J. M. O. Matos, B. O. Roos and P.-A. Malmqvist, *J. Chem. Phys.*, 1987, **86**, 1458–1466.

39 T. J. Penfold and G. A. Worth, *J. Chem. Phys.*, 2009, **131**, 064303.

40 E. B. Wilson, Jr., *Phys. Rev.*, 1934, **45**, 706–714.

41 Personal communications by E-mail.

42 F. Metz, M. J. Robey, E. W. Schlag and F. Dorr, *Chem. Phys. Lett.*, 1977, **51**, 8–12.

43 G. Fisher, S. Jakobson and R. Naaman, *Chem. Phys. Lett.*, 1977, **49**, 427–430.

44 N. Shimakura, Y. Fujimura and T. Nakajima, *Theor. Chim. Acta*, 1975, **37**, 77–88.

45 T. A. Stephenson, P. L. Radloff and S. A. Rice, *J. Chem. Phys.*, 1984, **81**, 1060–1072.

46 S. Kato, *J. Chem. Phys.*, 1988, **88**, 3045–3056.

47 D. M. Burland and G. W. Robinson, *J. Chem. Phys.*, 1969, **51**, 4548–4559.

48 H. Hornbnrger, *Z. Phys. D, At., Mol. Clusters*, 1988, **11**, 129–139.

49 S. H. Lin and R. Bersohn, *J. Chem. Phys.*, 1968, **48**, 2732–2736.

50 C. E. Otis, J. L. Knee and P. M. Johnson, *J. Phys. Chem.*, 1983, **87**, 2232–2239.

51 W. Siebrand, *J. Chem. Phys.*, 1966, **44**, 4055–4056.

52 B. R. Henry and W. Siebrand, *J. Chem. Phys.*, 1968, **49**, 5369–5376.

